ELSEVIER

Contents lists available at ScienceDirect

Materials Science & Engineering B

journal homepage: www.elsevier.com/locate/mseb



Highly stable full Heusler order Cs(Na, K)₂Bi with diverse topological phases controlled by strain engineering

Shahram Yalameha a, Zahra Nourbakhsh a, Ali Ramazani b, Daryoosh Vashaee c,d,*

- ^a Faculty of Physics, University of Isfahan, 81746-73441, Isfahan, Iran
- b Department of Mechanical Engineering, Massachusetts Institute of Technology, 77 Massachusetts Ave., Cambridge, MA 02139, USA
- ^c Department of Electrical and Computer Engineering, North Carolina State University, Raleigh, NC 27606, USA
- ^d Department of Materials Science and Engineering, North Carolina State University, Raleigh, NC 27606, USA

ARTICLE INFO

Keywords: Topological phases Topological insulator Weyl semimetal Spin-orbit coupling Strain-engineering

ABSTRACT

We predict the highly stable new full-Heusler order compound $Cs(Na, K)_2Bi$, that can take a diverse set of topological states by strain-engineering. Based on first-principles studies, our findings reveal that the hydrostatic lattice compression, uniaxial compression, and uniaxial tension can transition $Cs(Na, K)_2Bi$ to a trivial semiconductor, a normal insulator, a topological insulator, a Weyl semimetal, a Dirac semimetal, and a Nodal Line semimetal. These topological states, induced by various kinds of strain, exhibit a range of interesting optical and electronic transport properties. These results introduce $Cs(Na, K)_2Bi$ compounds as promising candidates to make novel topological devices whose properties can be controlled using strain-engineering.

1. Introduction

Design and discovery of topological quantum materials with exotic physical properties are some of the most challenging but fertile fields with revolutionary technological impacts [1]. If such materials are to underlay a technology, it is crucial to be able to control their topological phases systematically. A practical approach to control the topological phase conversion is based on strain engineering, where the symmetry and the electronic band structure can be controlled using an external stimulus.

In condensed matter physics, the classification of the phases of matter has played an essential role since Landau's theories, but in recent years the study of new phenomena, such as the quantum Hall effect [2], has led to a different classification paradigm based on the notion of topological order. The first realization of a topological material in solid-state and condensed matter physics has been the topological insulator (TI) [3-8], particular insulating systems in which the spinorbit coupling (SOC) provides a nontrivial topological order resulting in some unique properties [3,9], such as the presence of nontrivial metallic surface states, which are robust against disorder and other perturbations. In two-dimensions, Fermi contour, which can be defined on a surface, forms closed loops in k-space and, at some particular points called Dirac points, the surface states become doubly degenerate. In addition, away from these degenerate points that are called timereversal invariant momenta (TRIM) points, the low-energy dispersion becomes linear and form a conical intersection.

Very recently, another class of topological materials has attracted much attention because of their unique characteristics and properties, such as the topological Dirac semimetals (TDSM) [10], Weyl semimetals (TWSM) [11-16] and Nodal line semimetals (TNLSM) [17-20]. In the TI, the nontrivial topological characteristic comes out because of the SOC, while in contrast with the latter, the TDSM and TWSM present linearly dispersed low-energy excitation and the conical intersection at some unique momentum points of the bulk, a.k.a. Dirac or Weyl points, which usually do not appear on the TRIM points. The two-dimensions Fermi contour present on the surface now forms open lines in **k**-space, called Fermi arcs, whose endpoints are projections of two (or more) Dirac or Weyl fermion nodes on the surface of the Brillouin zone (BZ). The two nodes are characterized by having an opposite chirality, which acts as a source or sink of Berry curvature in k-space. Since they do not require any such symmetry-dependent protection, their topological properties are more robust than Dirac's ones. In the 3D band structure of TNLSM, it is allowed that bands can touch along a closed curve, which is called the nodal line. Such a nodal line can take the forms of a closed-loop or a chain consisting of several connected loops, i.e., nodal chain [21]. For TNLSM, this two-dimensional Fermi contour in k-space is called drum-head states.

The main difference between TDSM, TWSM, and TNLSM is symmetry breaking (SB). A TDSM, close to the Dirac node, has two-fold degenerate excitations. It generally requires three symmetries: time-reversal symmetry (TRS), inversion symmetry (IS), and an extra crystal

E-mail address: dvashae@ncsu.edu (D. Vashaee).

^{*} Corresponding author.

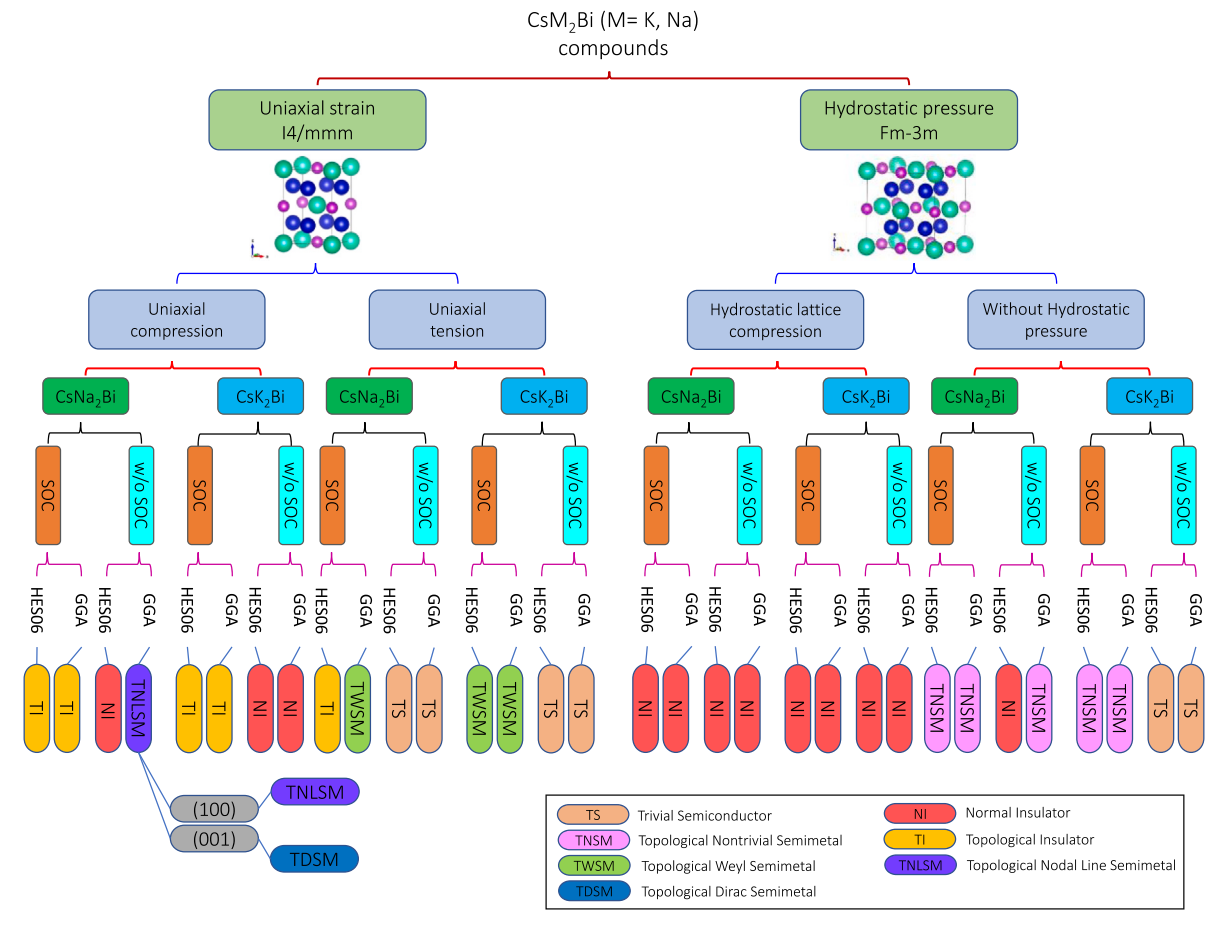


Fig. 1. Schematic illustrations of different topological classes of Full Heusler order compounds CsM₂Bi (M = Na, K), which can be effectively tuned by strain engineering. These compounds indeed show rich topological classes, ranging from TS, TNSM, TWSM, TDSM, NI, TI, and TNLSM. It should be noted that SOC and symmetry breaking by strain play essential roles in the emergence of these topological classes.

symmetry to be stable. But in a TWSM, the degeneracy is lifted by the breaking of either TRS or IS, and the nodes always come in pairs since they can be viewed as a Dirac node split in the k-space by the SB [22]. It is noteworthy that the TNLSM is protected by the dimension of nodes and certain symmetry. It can be classified into several groups. I) The nodal lines, which cross the BZ and end at the BZ boundary, can be stable states in the presence of SOC with the protection of non-symmorphic symmetry [23]. II) The closed-loop like nodal line, called the nodal circle state, can only be a stable state without SOC, and it is protected by TRS [19]. III) The nodal line circles can also be formed in non-centrosymmetric (or IS) crystals with mirror symmetry and survive even at the presence of SOC [24]. The TDSM, TWSM, and TNLSM exhibit novel quantum phenomena that are not only of interest for their fundamental physics but also may hold potential for technological applications such as quantum computing or low-energy spintronics devices [25].

Recently, it was realized that TWSM could be further categorized into three types according to the slope of band dispersion in the k-E space: type-I, type-II, and critical-type [18,26–28]. For type-I TWSM, the bands display conventional dispersions. In the type-II TWSM, the spectrum is tipped over, with electron and hole states coexisting at a given energy. The critical-type crossing is formed by a flat band and a dispersive band with the critical band dispersion between type-II and type-I. On the other hand, such classification has been extended to TNLSMs [18,19,26,29,30].

Topological quantum materials are mostly discovered in materials typically containing heavy elements where the band inversion is fundamentally based on the strength of the SOC. Therefore, the experimental demonstration of topological phases (TNLSM, TNLSM, and TDSM) have

been dominantly in the materials with strong spin–orbit interactions [14]. There has also been considerable interest in designing systems small or no SOC, with band inversions fulfilling the conditions of nontrivial topological phases [19,31]. The Dirac semimetal realized in A_3 Bi (A= Na, K, Rb) belongs to this class where the reversal of the band ordering between the conduction and valence bands is not ascribed to the SOC. In addition, the different topological phases observed in $Li_{3-x}Na_xM$ (x = 3, 2, 1, 0; M = N, P, As, Sb, Bi), and ABX (A = Sc, Zr, Hf; B = Co, Pt, Pd, Ir, Rh; X = Al, Ga, Sn) compounds in the presence and absence of SOC are also indicative of this matter [14,20,32,33].

Since discovering topological insulators and nontrivial materials, there have been significant efforts to find the compounds representing the various topological classes. The current high-throughput search methods can categorize materials based on their band structure and topological indexes [34-36]. The motivations behind high-throughput calculations are to screen the materials and find the ones with nontrivial phases. However, such high-level analyses do not identify the specific topological phases, nor do they calculate many critical material properties, necessitating more detailed investigations. Many materials listed in the databases developed by high-throughput calculations are also unstable and cannot be practically realized. This matter explains why many materials (20%~30% of the crystal database materials) are found to be nontrivial topological. Moreover, it is critical, for technical purposes, to identify means to control and tune the topological phases systematically. Therefore, the materials diagnosed by the high-throughput searches still have to be investigated, theoretically or experimentally, to confirm and identify the topological phases, check their stability, and find methods to control their topological properties.

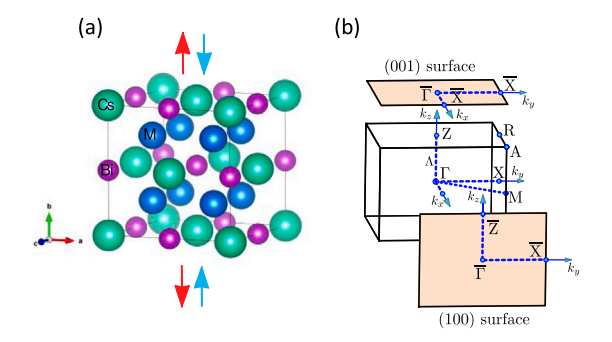


Fig. 2. Crystal structure and Brillouin zone (BZ). (a) The conventional crystal structure for CsM_2Bi (M = Na, K) compounds with space group Fm-3m (No. 225). Red and blue arrows indicate uniaxial tensile and compression strains, respectively. (b) Schematic of the bulk BZ and its projection onto (001) and (100) surfaces with high symmetry points. (For interpretation of the references to color in this figure legend, the reader is referred to the web version of this article.)

In this regard, studies, such as the current work, provide more comprehensive information to better evaluate a materials system for practical realization and device application.

There have been several reports on the role of the strain on topological phases, which showed in some materials, a strain can modify the bandstructure; hence, the topological phase. [37–40]. Many such works are focused on monolayers or are limited to one kind of strain resulting in a single topological phase. There is no prior work that introduces material that can take various nontrivial topological phases depending on the type of strain, e.g., uniaxial or biaxial compression/tension or hydrostatic lattice compression. Furthermore, it is important to know if the required strain is small enough to be practically feasible from a technical perspective.

In this paper, using first-principles density functional theory (DFT), we predict the new compounds of CsM2Bi (M = Na, K), zero-gap semimetals with an inverted band structure, which can be driven into different topological classes by strain engineering. Furthermore, we will show that these compounds take the cubic space group Fm-3m (No. 225) in a full Heusler-type structure. As such, although they do not share some of the common properties of the full Heusler alloys, we will refer to their structure as full Heusler order (FHO) in the manuscript. These structures, by strain engineering, show rich topological classes, ranging from trivial semiconductor (TS), topological nontrivial semimetal (TNSM), TWSM, TDSM, normal insulator (NI), topological insulator (TI) and TNLSM (see Fig. 1). It should be noted that the presence or absence of SOC, symmetry breaking, induced by a uniaxial strain, and exchange-correlation functional play essential roles in the emergence of these topological classes. Furthermore, we investigate the phonon dispersion and the elastic constants systematically. Finally, we show that these materials are dynamically and mechanically stable, making them promising candidates for practical applications.

2. Computational details

Our calculations are carried out in the framework of DFT by using the WIEN2K package [41]. The generalized gradient approximation (GGA) of Perdew–Burke Ernzerhof (PBE) formalism [42], and Heyd–Scuseria–Ernzerhof (HSE06) hybrid [43] are adopted for the exchange-correlation potential. The bulk BZ of these compounds is calculated using an $11\times11\times11$ k-point mesh. To get the tight-binding model Hamiltonian, we used the WANNIER90 package [44] to obtain maximally localized Wannier functions. Finally, the resulting tight-binding model was computed for the surface spectral functions, $\rho(E,k)$, in a semi-infinite geometry, using an iterative Green's function method [45]. Here $\rho(E,k) = -Tr[G_{00}(E,k)]/\pi$, where $G_{00}(E,k)$ is the Green's function corresponding to the surface layer. The phonon dispersion of CsM₂Bi material is computed using the PHONOPY code [46]. For elastic constants calculations, we used the IRELAST code [47].

3. Results and discussion

3.1. Structural, mechanic, and dynamic equilibrium properties

The crystal structure of FHO CsM₂Bi (M = Na, K) (from the family of bialkali bismuthide compounds) has the cubic shape with space group Fm-3m (No. 225), as shown in Fig. 2(a). The optimized values of the primitive lattice constants (a_0) of these compounds are 5.870 Å (CsNa₂Bi) and 6.320 Å (CsK₂Bi). No experimental or theoretical evaluation has been performed on these structures, but as we will discuss, they have excellent mechanical and dynamic stability. The calculated elastic constants, namely, (C₁₁, C₁₂, C₄₄), of CsNa₂Bi and CsK_2Bi with the cubic system, are (29.58, 7.24, 12.37) GPa and (14.05, 7.85, 10.25) GPa, respectively, and satisfy the Born-Huang mechanical stability criteria for the cubic system [48]. C_{11} (= C_{22} and C₃₃) represent the uniaxial deformation along the [100] ([010] and [001]) crystallographic direction [49]. As such, the uniaxial deformation resistance of CsNa2Bi is more than CsK2Bi. This effect is apparent when a uniaxial lattice compression is applied to calculate the electronic band structure (see Section 3.4).

Phonon dispersion studies are fundamental in underpinning the vibrational dynamics in a phase transition and the practical feasibility to synthesize the material. Therefore, dynamic stability is of very high importance for evaluating the stability of new materials. We calculated the phonon dispersion curves as a function of the lattice constant (LC), as shown in Fig. 3. It should be noted that SOC effects are considered in these calculations. It can be seen that the phonon dispersion exhibits no imaginary frequency (soft phonon modes) in the equilibrium LC, confirming the dynamic stability of these compounds. With increasing the LC up to 2.4% (e.g., by temperature or hydrostatic pressure), the soft modes appearing in the CsNa₂Bi at X point show a phase transition (Fig. 3(a)). There is no such behavior in the CsK₂Bi by increasing the LC up to 1.58% (Fig. 3(b)). However, as the LC increases by up to 2.7% in CsK,Bi, the soft modes also appear at X point.

3.2. Equilibrium electronic structure the presence and absence of SOC

Firstly, we focus on the electronic band structures of these compounds in the presence and absence of SOC. As shown in Fig. 4, we discuss the TS, TNSM, and NI classes that appear in these compounds in this section. We first investigate the electronic structure of CsNa₂Bi. Fig. 4(a) presents the energy band structure of CsNa₂Bi within GGA and HSE06 approaches with and without SOC along the M-G(Gamma)-X path. In the absence of SOC within the GGA approach, it shows a zerogap semimetal band structure. However, there is an apparent nontrivial bandgap (6.7 meV), below the Fermi energy (marked in green color) that represents the topological nontrivial semimetal (TNSM) phase. Moreover, from the projected band structures in Fig. 4(d), we confirmed the s-p band inversion, with Bi-s-liked below Bi-p-liked band. If we look at the HSE06 approach of band structure (red color), the CsNa₂Bi is a semiconductor with a direct trivial bandgap of 0.38 eV (Fig. 4(b)). Therefore, it can be considered in the "Normal insulator (NI)" topological class. The electronic band structure with GGA and HSE06 approaches of CsNa2Bi after considering SOC is also shown in Fig. 4(b). We can clearly find that this compound is a zero-gap semimetal within both approaches, and has a nontrivial band gap below the Fermi energy (0.56 eV in the GGA and 0.48 eV in the HSE06 methods). It is noteworthy that in this case, the gapless point at G (Gamma) near Fermi energy is protected by time-reversal symmetry. The projected band structure in Fig. 4(d), also shows the s-p band inversion at G-point. Therefore, we classify CsNa₂Bi as a TNSM in both approaches. Next, we consider the CsK₂Bi structure. In the absence of SOC, CsK₂Bi is a semiconductor with 0.29 eV (0.72 eV) bandgap within the GGA (HSE06) approach (Fig. 4(c)). Fig. 4(e) also confirms that there is no band inversion (Bi-p-liked below Bi-s-liked band). Thus, we classify CsK2Bi as a trivial semiconductor (TS) within both

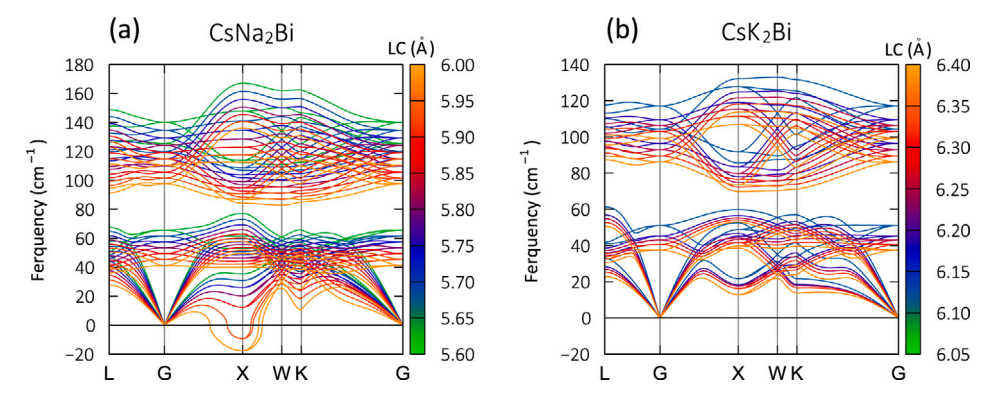


Fig. 3. The calculated phonon dispersion curve of (a) CsNi₂Bi and (b) CsK₂Bi compounds. Phonon dispersion curves are plotted as a function of lattice constant (LC). The soft modes appear in the CsNa₂Bi at X point, upon 2.4% LC increasing, indicating a phase transition. It should be noted that in these calculations, SOC effects are considered.

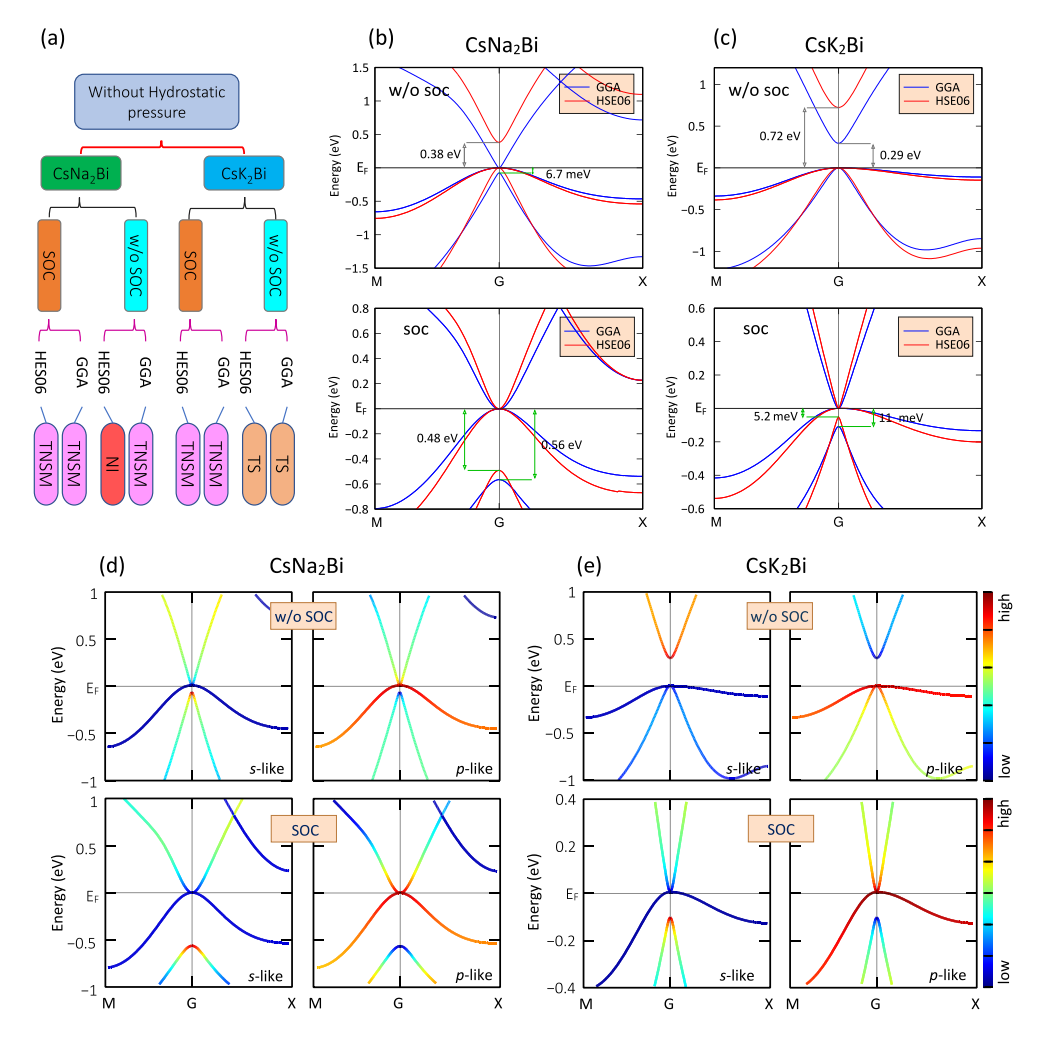


Fig. 4. (a) Schematic illustrations of different topological classes of CsM_2Bi (M = Na, K) compounds at zero hydrostatic pressure, which includes TS, TNSM and NI classes. (b) and (c) Equilibrium electronic structure of CsM_2Bi calculated with and without SOC in GGA and HSE06 approaches. Nontrivial band gaps are marked with green arrows. (d) and (e) The projected band structure with and without turning on SOC based on the GGA approach. The projected band structure shows the s-p band inversion at G-point. Due to the similarity of the results, only GGA results are shown here.

approaches. When we include SOC in the calculations, a nontrivial band gap about 11 meV (5.2 meV) in the GGA (HSE06) approach opened below the Fermi energy, which creates an s-p band inversion (Fig. 4(e)). Therefore, it is concluded that CsK_2Bi , similar to $CsNa_2Bi$, is classified as TNSM within both approaches.

Topological surface states (TSS) are prime characteristics of the topological materials that reflect the bulk-boundary correspondence [50]. The calculated TSS for the semi-infinite (001) surface of $CsNa_2Bi$

and CsK_2Bi are shown in Fig. 5 (due to the similarity of the results, only the TSS with the GGA approach in the presence of SOC are shown in the figure). Since the band inversion occurs below the Fermi energy, the TSS is calculated below the Fermi energy. In addition, the TSS with a Dirac-type crossing is inside the projected valence bands due to the mixing with bulk electronic states. The blue arrow shows the Dirac point.

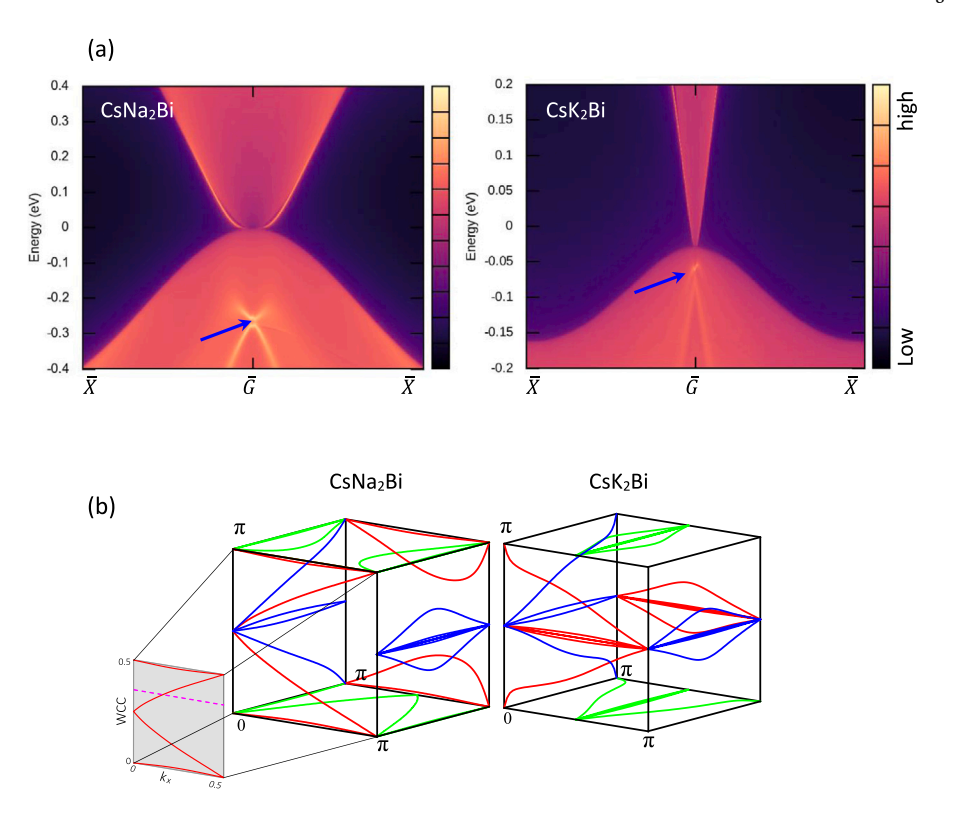


Fig. 5. (a) The calculated TSS for the semi-infinite (001) surface of $CsNa_2Bi$ and CsK_2Bi . The TSS with a Dirac-type crossing is inside the projected valence bands due to the mixing with bulk electronic states. The blue arrow shows the Dirac point. Due to the similarity of the results, the surface band structures with the GGA approach considering the SOC are shown in this figure. (b) Time reversal invariant cube (TRIC). The WCC evolution for CaM_2Bi compounds on six time-reversal invariant momentum plane, $k_x = 0$, π (red color), $k_y = 0$, π (blue color) and $k_z = 0$, π (green color). The arbitrary reference line (pink line) is shown for $k_x = 0$ plane. (For interpretation of the references to color in this figure legend, the reader is referred to the web version of this article.)

The topological invariants are essential to characterize a material into topological classes. There are different methods to obtain topological invariants. For example, the product of eigenvalues parities is calculated at TRIM points [51], or the Wilson loops around the Wannier Charge Centres (WCC) are calculated [52]. In this work, we used the WCC method, and for this purpose, we have included the sixtime reversal invariant planes (TRIP) in a cube called the time-reversal invariant cube (TRIC) (Fig. 5(b)). The topological invariants (v_0 ; v_1 , v_2 , v_3) computation is carried out along the six TRIP $k_x = 0$, π , $k_y = 0$, π and $k_z = 0$, π in the BZ, which are included in TRIC. Therefore, the topological invariants (v_0 ; v_1 , v_2 , v_3) are computed using equation, v_0 = $(ARL (k_i = 0) + ARL (k_i = \pi)) \mod 2$ and $v_i = ARL (k_i = \pi) \mod 2$. To calculate the ARL, one draws an arbitrary reference line parallel to the TRIP axis and counts the number of times the WCC crosses this line. An arbitrary reference line for $k_x = 0$ plane, as an example, is shown in Fig. 5(b) (pink line). Based on these explanations, CsM_2Bi (M = Na, K) are characterized by (1; 0,0,0) or $Z_2 = 1$, which means both compounds are strong nontrivial topological material in the equilibrium state.

3.3. The electronic structure under hydrostatic pressure in the presence and absence of the SOC

The topological properties of CsM_2Bi can change by applying external hydrostatic pressure. As we will show, both compounds show semimetal electronic band structures under hydrostatic lattice compression. Hence, they can be classified as normal insulators or trivial insulators [53] in terms of the topological class (Fig. 6(a)). Increasing the pressure (hydrostatic lattice compression) opens up a new trivial band gap between the valence and conduction bands. In this case, we show that the hydrostatic lattice compression leads to the topological phase transition from nontrivial to trivial topological phase. When SOC within GGA approach is considered, at $V/V_0 \approx 0.85$ ($V/V_0 \approx$

0.94) CsNa₂Bi (CsK₂Bi) compound is converted into semiconductor with 4.6 meV (2.7 meV) bandgap. Considering the HSE06 approach, the bandgap of CsNa₂Bi (CsK₂Bi) increases to 0.1 eV (7.6 meV) (see Fig. 6(b) and (c)). When SOC is neglected, we have similar results, and only the bandgap is increased, as shown in Fig. 6(b) and (c).

To confirm that the trivial band gaps appear in these structures under hydrostatic pressure, we calculated the projected band structure, as shown in Fig. 6(d) and (e). From the structure of the band provided in these figures, it can be seen that the band inversion does not occur. The Bi-s-liked is above the Bi-p-liked bands. This result is valid within both approaches; thus, only the results of the GGA approach are shown in Fig. 6(d) and (e). We further verify that TSS does not appear in these conditions, and the topological invariants are (0; 0,0,0). These results are included in Fig. 7. According to Fig. 7(a), we can observe that the TSS does not appear in the area where there is a trivial bandgap. Also, according to the TRIC in Fig. 7(b), the value of ARL $(k_i = 0) + ARL (k_i = \pi)$ is even, and as a result, v_0 becomes zero $(Z_2 = 0)$.

3.4. The electronic structure under uniaxial strain in the presence and absence of the SOC

In this section, we show that the compounds have different responses to the topological properties under compression and tension. Under uniaxial tension, the materials become TWSM and TS (see Fig. 11(a)). However, the uniaxial compression converts these compounds into TI, NI, and even TDSM or TNLSM (Fig. 8(a)). When we impose a uniaxial strain (compression or tension) along any orthogonal axis (here the c axis) on the original Fm-3m structure, it will change the symmetry of the crystal (breaking the cubic symmetry) from space group Fm-3m to I4/mmm. To keep the volume of the cell invariable, when a tensile (compressive) strain, μ , is applied along the c axis, we add a compressive (tensile) strain $1/\sqrt{(1+\mu)}$ along with the a and b

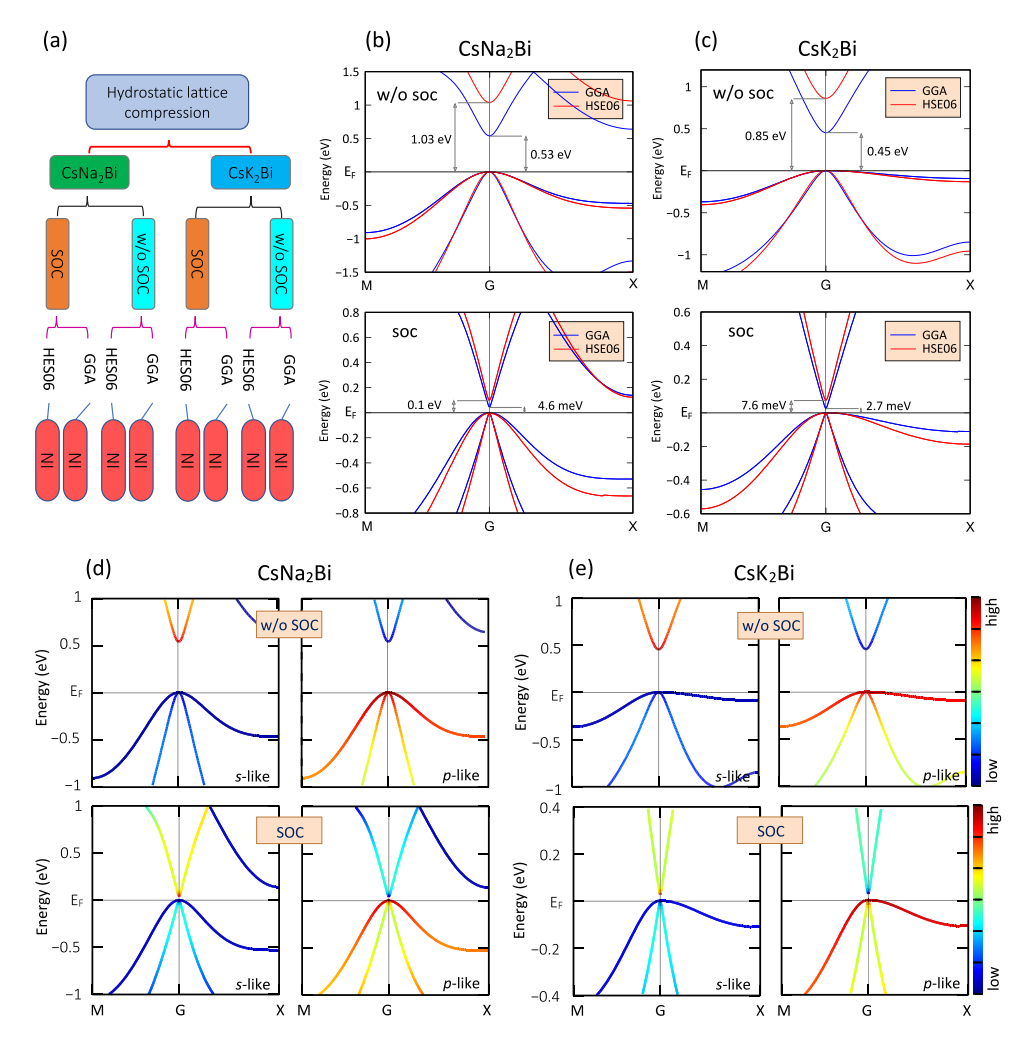


Fig. 6. (a) Schematic illustrations of different topological classes of CsM₂Bi (M = Na, K) compounds under hydrostatic pressure. We can observe that these compounds all show semimetal electronic band structures under hydrostatic lattice compression. Hence, these compounds can be classified as normal insulators (NI) or trivial insulators in terms of topological class. (b) and (c) show the electronic structure of CsM₂Bi calculated without and with the SOC within GGA and HSE06 approaches. Increasing the pressure opens up a new trivial band gap between the valence and conduction bands. (d) and (e) show the projected band structure with and without turning on the SOC effect within the GGA approach. It can be seen that the band inversion does not occur as the Bi-s-liked is above the Bi-p-liked.

axes, respectively. To cover more details, we divide this section into two sub-sections.

Uniaxial compression. It was explained at the beginning of Section 3.1 that the uniaxial deformation resistance of CsNa2Bi is more than CsK2Bi. Therefore, the compressive strain in the CsK2Bi is easier to obtain than in the CsNa2Bi compound. As such, the topological properties of CsNa₂Bi and CsK₂Bi appear at 1.58% ($c = a_0 - 1.58\% a_0$) and 2.06% ($c = a_0 - 2.06\% a_0$) strain, respectively. The band structures of CsNa2Bi within GGA and HSE06 approaches are presented in Fig. 8(b). Before considering the SOC, the band structure in the GGA approach shows that there is a band crossing (gap-less point) in the G-X path while a small bandgap (1.4 meV) appears in the G-Z path. Although we have a small bandgap in the G-Z path, and we seem to have a type-I TWSM, the calculations of TSS show that the TSS is drum-head-like surface states (DHLSS) (this matter will be examined). This indicates that CsNa₂Bi is type-I TNLSM within the GGA approach in the absence of SOC. This type-I TNLSM is protected by time-reversal symmetry and the mirror symmetry M_z. It is noteworthy that by increasing the uniaxial compression, the bandgap can be closed. In addition, the presence of bandgaps in TNLSM compounds has been observed [20,54,55]. If the HSE06 approach is used, it can be seen that CsNa₂Bi is a semiconductor with 36 meV bandgap, which is classified in the trivial topological classes or NI. Since the band structure in the GGA approach is more credible, the projected band structure is calculated

with GGA approach in the absence of SOC and shown in Fig. 8(d). When a uniaxial compression breaks the cubic symmetry, the degeneracy of the G point bands is lifted. The band splitting between the valence Bi- $p_{x,y}$ -like states, and the conduction creates at the G point is composed mainly of Bi- p_z -like states. Since the p_z - $p_{x,y}$ type band inversion at the G point is preserved, the phase remains topologically nontrivial. This type of band inversion in the KNa₂Bi under uniaxial strain has also been observed in the past [56]. When we include the SOC in the calculations (GGA and HSE06 approaches) for CsNa₂Bi, a new nontrivial bandgap opens, as shown in Fig. 8(b). Also, there is p_z - $p_{x,y}$ type band inversion at G points, as shown in Fig. 8(d). This band inversion stems from the on-site energy difference between the p_z -orbital and $p_{x,y}$ -orbital (the Bi- p_z -like is above the Bi- $p_{x,y}$ -liked band). This band inversion with a nontrivial bandgap induces the topologically nontrivial properties so that they can be classified into a TI class.

The band structure of CsK_2Bi within the GGA and HSE06 approaches in the presence and the absence of SOC is depicted in Fig. 8(c). It is seen that CsK_2Bi is a semiconductor with a trivial band gap of 32 meV (70 meV) within the GGA (HSE06) approach when the SOC is turned off. According to the projected band structure with and without turning on the SOC effect based on the GGA approach in Fig. 8(e), it is observed that the p_z – $p_{x,y}$ type band inversion has not occurred. It can be concluded that CsK_2Bi is a NI in the absence of SOC. It is noteworthy that due to the similarity of the band structures of these compounds

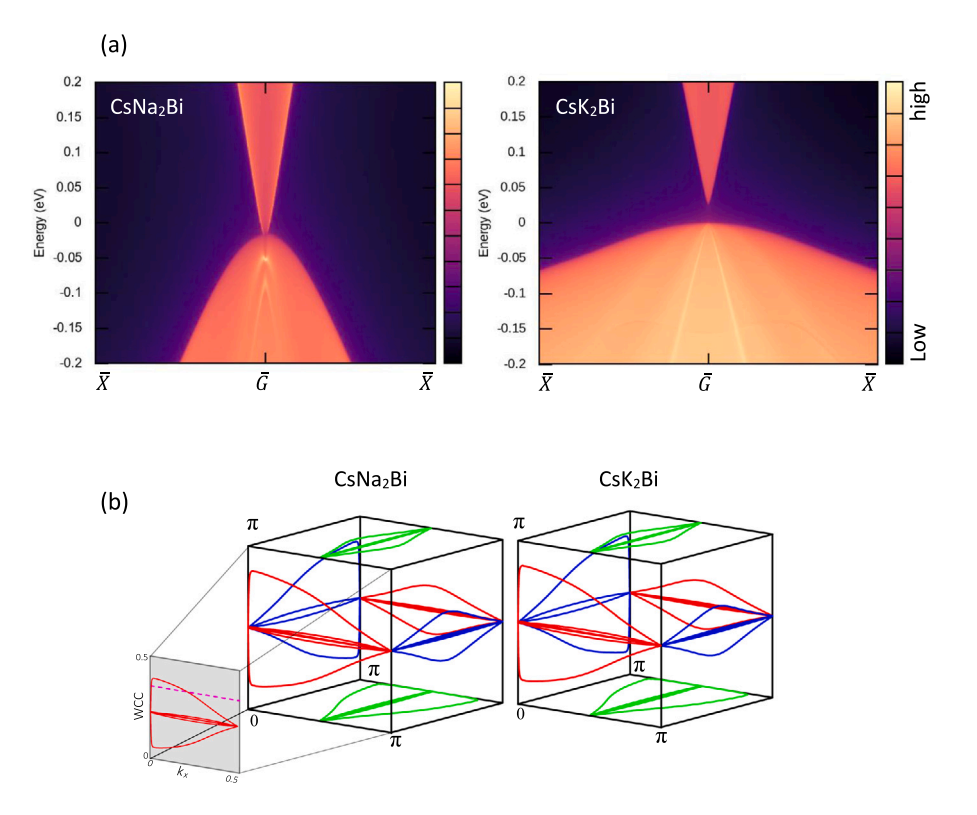


Fig. 7. (a) The calculated TSS for the semi-infinite (001) surface of $CsNa_2Bi$ and CsK_2Bi . The TSS does not appear in the area where there is a trivial band gap is. Due to the similarity of the results, the surface band structures within the GGA approach and in the presence and absence of SOC are shown in this figure. (b) Time reversal invariant cube (TRIC). The WCC evolution shows for CaM_2Bi compounds on six time-reversal invariant momentum plane, $k_x = 0$, π (red color), $k_y = 0$, π (blue color) and $k_z = 0$, π (green color). The arbitrary reference line (pink line) shows for $k_x = 0$ plane. (For interpretation of the references to color in this figure legend, the reader is referred to the web version of this article.)

within different approaches, only the projected band structure with the GGA approach is included in Fig. 8(e). For CsK_2Bi , when SOC is taken into account, a small gap opens at the G point, driving the system into a narrow-gap TI, similar to the results of $CsNa_2Bi$ within GGA and HSE06 approaches. (Fig. 8(c)). In this case, the p_z – $p_{x,y}$ type band inversion also occur (see Fig. 8(e)).

According to the bulk boundary correspondence, as discussed in the previous sections, the TSS, in this case, is also expected to appear on the surface of these materials. To show these TSS, we calculated the surface states, as shown in Fig. 9(a) and Fig. 10(a) for (001) surface, and in Fig. 9(b) and Fig. 10(b) for (100) surface. When the SOC is ignored, DHLSS appears near the G point in the (100) surface, but a TDSM in the (001) surface. To confirm DHLSS, we calculated the surface states at different energy values, as shown in Fig. 9(c). In this figure, we can clearly find that there exist DHLSS in the CsNa2Bi in the absence of SOC. When SOC is included, CsNa2Bi becomes TI, with TSS at both (001) and (100) surfaces, as shown in Fig. 10(a) and (b). In addition, in Fig. 10, we plotted the projection of the surface states on the (100) and (001) planes, which clearly shows the presence of TSS. Another characteristic feature of topological surface state is the helical spin texture. To study this feature, we calculate the spin texture for one of the surfaces (i.e., (100) surface), as shown in Fig. 10(c). On this surface the spin texture in the upper part of the Dirac cone is strongly warped. This is due to the lack of C4-symmetry, which has also been observed in other topological materials, such as KNa2Bi [56].

Uniaxial tension. We investigated the topological properties, and the corresponding band structures of the $CsNa_2Bi$ (CsK_2Bi) compound in the presence of SOC within the GGA and HSE06 approaches under a uniaxial tension of 0.95% ($c=a_0+0.95\%a_0$) (0.30% ($c=a_0+0.30\%a_0$)) (see Fig. 11(a)). These tensile values close the energy gap created in the compression strain. The results are shown in Fig. 11(b) (Fig. 11(c)).

As shown in Fig. 11(c), we can find that, without considering the SOC, CsNa₂Bi is a zero-gap semimetal within the GGA approach, while it is a semiconductor with a bandgap of 0.28 eV within the HSE06 approach. In the HSE06 approach, CsNa2Bi is a trivial semiconductor (there is no p_z – $p_{x,y}$ type of band inversion not shown in the figure due to the similarity to the previous data of this type band inversion), However, within the GGA approach, it appears that the composition can be a TNLSM or a TWSM. Therefore, we will examine the projected band structure in more detail. As shown in Fig. 11(d), there appears to be a band inversion at the crossing point in the Z-G path (green arrow), but given Fig. 11(f), it is clear that at G point, there is a crossing point between the conduction band and the valance bands (green and blue colors). However, there is no band inversion between these bands. Therefore, in this approach, the CsNa2Bi is a TS. The band structure after considering SOC within the GGA approach Fig. 11(b) shows that the two-fold degenerate valence band crosses with the conduction band on the Z-G path and forms Dirac nodes (Weyl points). The band inversion in Fig. 11(d) of the nontrivial phase confirms this case, similar to KNa₂Bi [56]. As shown in Fig. 11(b), when the band structure is calculated within the HSE06 approach in the presence of SOC, the CsNa₂Bi compound is a semiconductor with a nontrivial band gap above 0.06 eV. Since this band inversion is similar to Fig. 8(d), such as we consider CsNa2Bi in this approach in the TI class.

The band structures of the CsK_2Bi with and without SOC are shown in Fig. 11(c). In the absence of SOC, we can see that this compound has semiconductor band structures with trivial band gaps of 0.28 and 0.65 eV within GGA and HSE06 approaches, respectively. To confirm these trivial band gaps, we calculated the projected band structure within the GGA approach (HSE06 approach is similar to GGA approach) in Fig. 11(e). As shown in this figure, the band inversion does not occur; thus, this compound is a trivial phase (TS) in the absence of SOC within both approaches. In the presence of the SOC, such as the

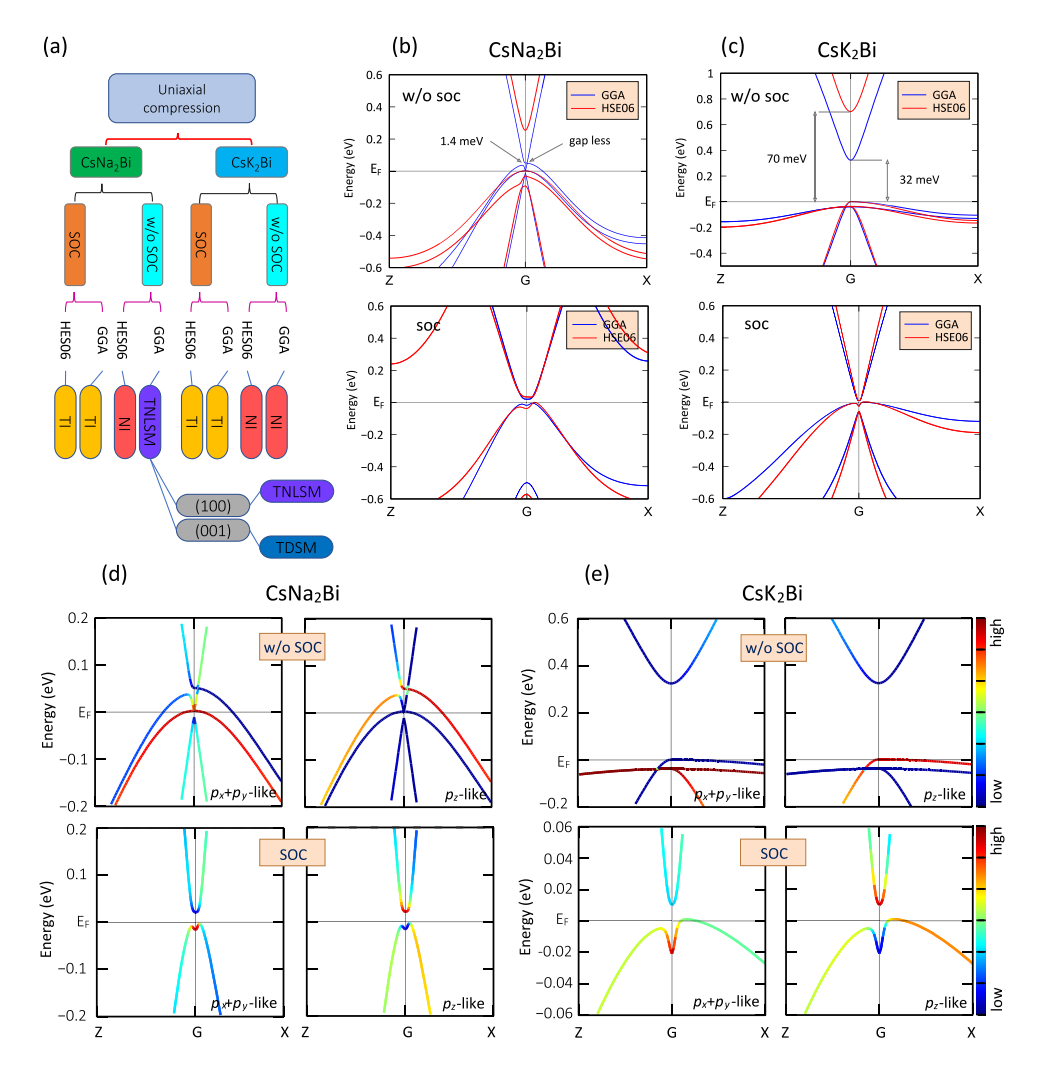


Fig. 8. (a) Schematic illustrations of different topological classes of CsM_2Bi (M = Na, K) compounds under uniaxial compression. The uniaxial compression converts these compounds into TI, NI, and even TDSM or TNLSM. (b) and (c) Electronic band structure of CsM_2Bi calculated without and with SOC within GGA and HSE06 approaches. (d) and (e) show the projected band structure with and without turning on the SOC effect based on the GGA approach.

case of CsNa₂Bi, the two-fold degenerate valence band crosses with the conduction band on the Z–G path and form Dirac nodes (Weyl points) for the CsK₂Bi (as shown in Fig. 11(c) and Fig. 11(e) by black arrow).

The Dirac nodes and the inverted band order in the presence of SOC suggest the existence of nontrivial surface states, namely the Fermi arcs. On the other hand, if the system has an additional C_n , in particular, C3, C4, and C6 rotation symmetries, the rotation symmetry can protect the band crossing at specific generic discrete points, turning the system into a TWSM [17,56]. There is C₄ rotation symmetry in these structures. Therefore, the corresponding nontrivial surface states of these compounds, connecting the Dirac nodes, emerge in the (100) and (001) surfaces, as shown in Fig. 12. Fig. 12(a-d) shows the projection of the Dirac nodes of CsNa₂Bi and CsK₂Bi onto the (001) and (100) surfaces of the BZ, demonstrating the existence of the characteristic Fermi arcs (FA) of the TWSM. The FA surface states of CsK₂Bi are similar to CsNa₂Bi and are not included in this figure. The Fermi surface is composed of two half-circle FAs closed with two singular Weyl points (blue and green points) corresponding to the projection of bulk Dirac nodes. In addition, to clearly show the Weyl point, spin texture, and Berry curvature of one of these compounds, CsNa2Bi, are calculated, and the results are shown in Fig. 13(a) and (b). As known, the Weyl point behaves as a magnetic monopole [57,58], which is a source or sink of the Berry curvature in the bulk band structures. These source and sink points are the Weyl points with positive and negative chirality, and they can be identified in the Berry curvature, as shown in Fig. 13(a). The

spin texture of Fermi arcs has a helical behavior, for which the value of the spin is not defined at the Weyl points [56]. This feature is well illustrated in Fig. 13(b). Finally, the topological invariant, (1; 0,0,0), identified by the TRIC in Fig. 13(c) indicate that both structures have the nontrivial phase in the presence of SOC. At the end of this section, to describe the change in the band dispersion around the G point under pressure (3.3 and 3.4 Secs.), we have constructed a low-energy effective k-p model Hamiltonian in which the C $_4$ rotation, TR, and the inversion symmetries are considered. In this model, only low-energy electronic states around the G point, which are mostly consisted of p-Bi orbitals, are used as the basis states [56], and the coupling of the basis states, i.e., p-orbital hybridization, with the same parity is also accounted. Based on this basic set, the Hamiltonian can be written as,

$$H(\mathbf{k}) = \begin{pmatrix} M(\mathbf{k}) & \alpha k_z (k_x + i k_y) & 0 & B^*(\mathbf{k}) \\ \alpha k_z (k_x - i k_y) & -M(\mathbf{k}) & B^*(\mathbf{k}) & 0 \\ 0 & B(\mathbf{k}) & M(\mathbf{k}) & -\alpha k_z (k_x - i k_y) \\ B(\mathbf{k}) & 0 & -\alpha k_z (k_x + i k_y) & -M(\mathbf{k}) \end{pmatrix};$$
(1)

where $M(k) = m_0 - m_1 k_z^2 - m_2 (k_x^2 + k_y^2)$ and $B(k) = \beta (k_x + i k_y)^2$. The parameters of the low-energy effective k-p model are m_0 , m_1 , m_2 , α , and β . m_1 , m_2 , α , and β parameters are fixed in our calculation ($m_1 = 1.1$ eV Å, $m_2 = -1.0$ eV Å, $\alpha = 1.1$ eV Å and $\beta = 1.0$ eV Å) to reproduce the topological phase transition. Therefore, the only variable

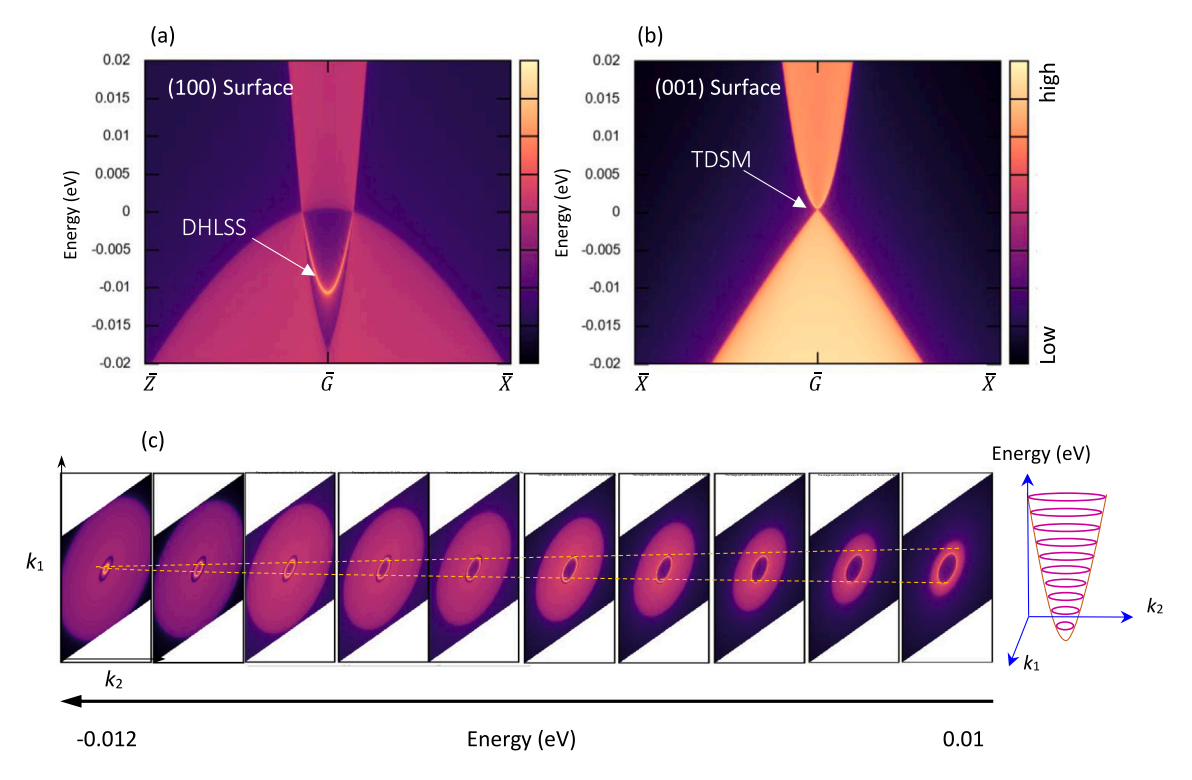


Fig. 9. The calculated TSS for the semi-infinite (a) (100) surface and (b) (001) surface of $CsNa_2Bi$ without SOC, when SOC is ignored, DHLSS appear near the G point in the (100) surface, while a TDSM appears in the (001) surface. (c) The surface states projected onto (100) surface at different energy values. It can be seen that there exists DHLSS in the $CsNa_2Bi$ in the absence of SOC.

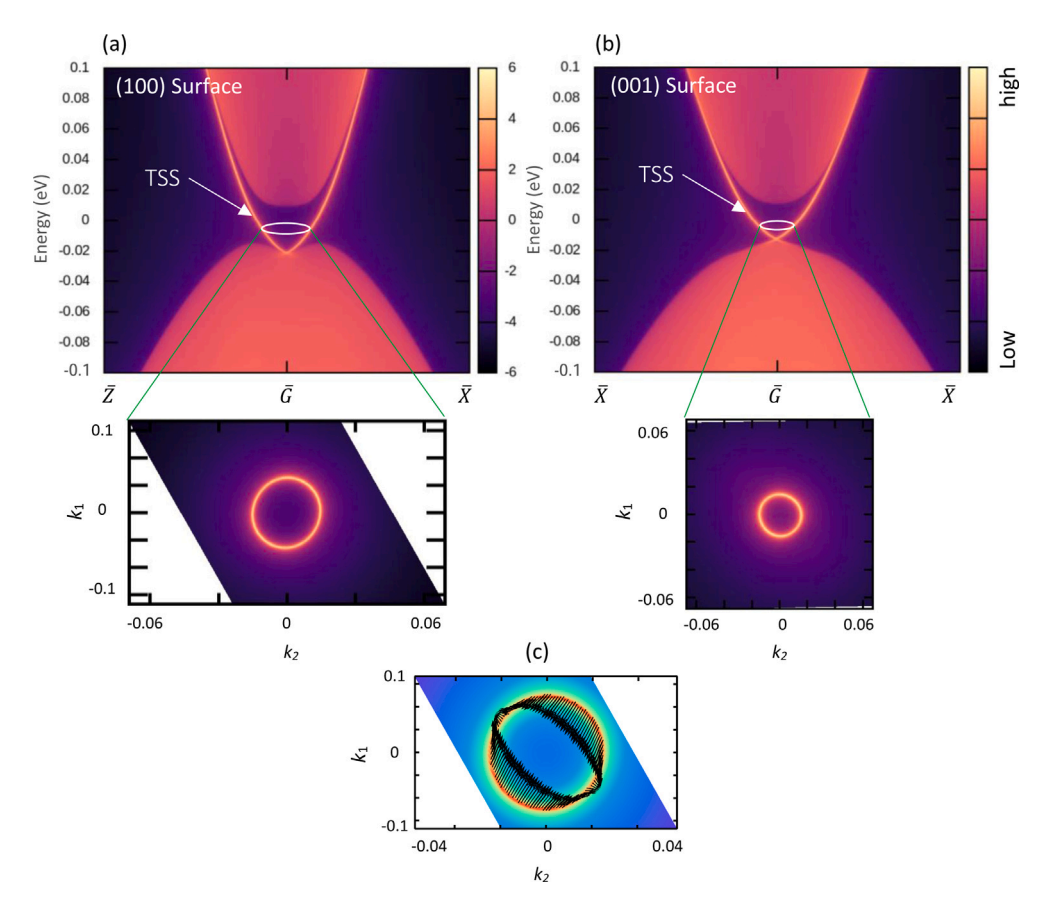


Fig. 10. The calculated TSS for the semi-infinite (a) (100) surface and (b) (001) surface of $CsNa_2Bi$ with SOC. When SOC is taken into account, the material becomes TI, with TSS at both (001) and (100) surfaces. The projection of the surface states on the (100) and (001) planes shows the presence of TSS clearly. (c) Spin texture of $CsNa_2Bi$ in the upper part of the Dirac cone on the (100) surface. On this surface, the spin texture in the upper part of the Dirac cone is strongly warped due to the lack of C_4 symmetry.

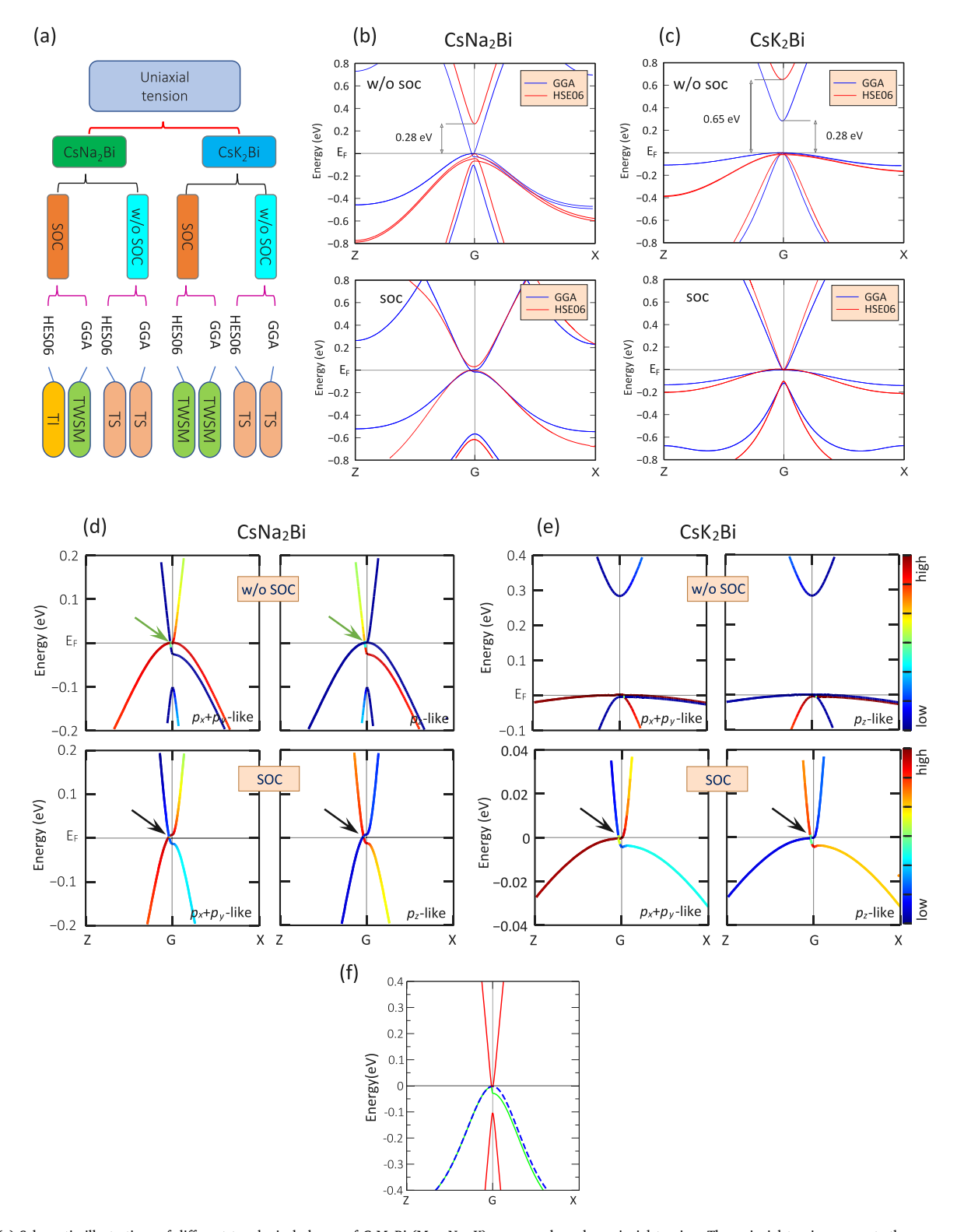


Fig. 11. (a) Schematic illustrations of different topological classes of CsM_2Bi (M = Na, K) compounds under uniaxial tension. The uniaxial tension converts these compounds into TI, TS, and even TWSM. (b) and (c) shows the electronic band structure of CsM_2Bi calculated with and without SOC in GGA and HSE06 approaches. (d) and (e) The projected band structure with and without turning on the SOC effect based on the GGA approach. (f) shows the electronic band structure of CsM_2Bi calculated without SOC.

parameter for investigation of the Hamiltonian and the topology of the band structure is m_{0} , which corresponds to the energy difference between the basis orbitals. Hence, the spectra of Hamiltonian(E(k)) are obtained as follows,

$$E(\mathbf{k}) = \pm [m_0 - m_1 k_z^2 - m_2 (k_x^2 - k_y^2) + \beta^2 (k_x + i k_y)^2 (k_x - i k_y)^2$$

$$+ \alpha^{2}(k_{x} + ik_{y})(k_{x} - ik_{y})k_{z}^{2}]^{1/2}.$$
 (2)

The $E(\mathbf{k})$ is calculated for different values of m_0 , as shown in Fig. 14. When m_0 =0, the compound is a zero-gap semimetal (Fig. 14(b)). Two double degenerate bands along with all the directions of the BZ ([1,0,0]-[0,0,0]-[0,0,1] in the figure) are touching at the G, point and the crossing point has a four-fold degeneracy. This case is compatible

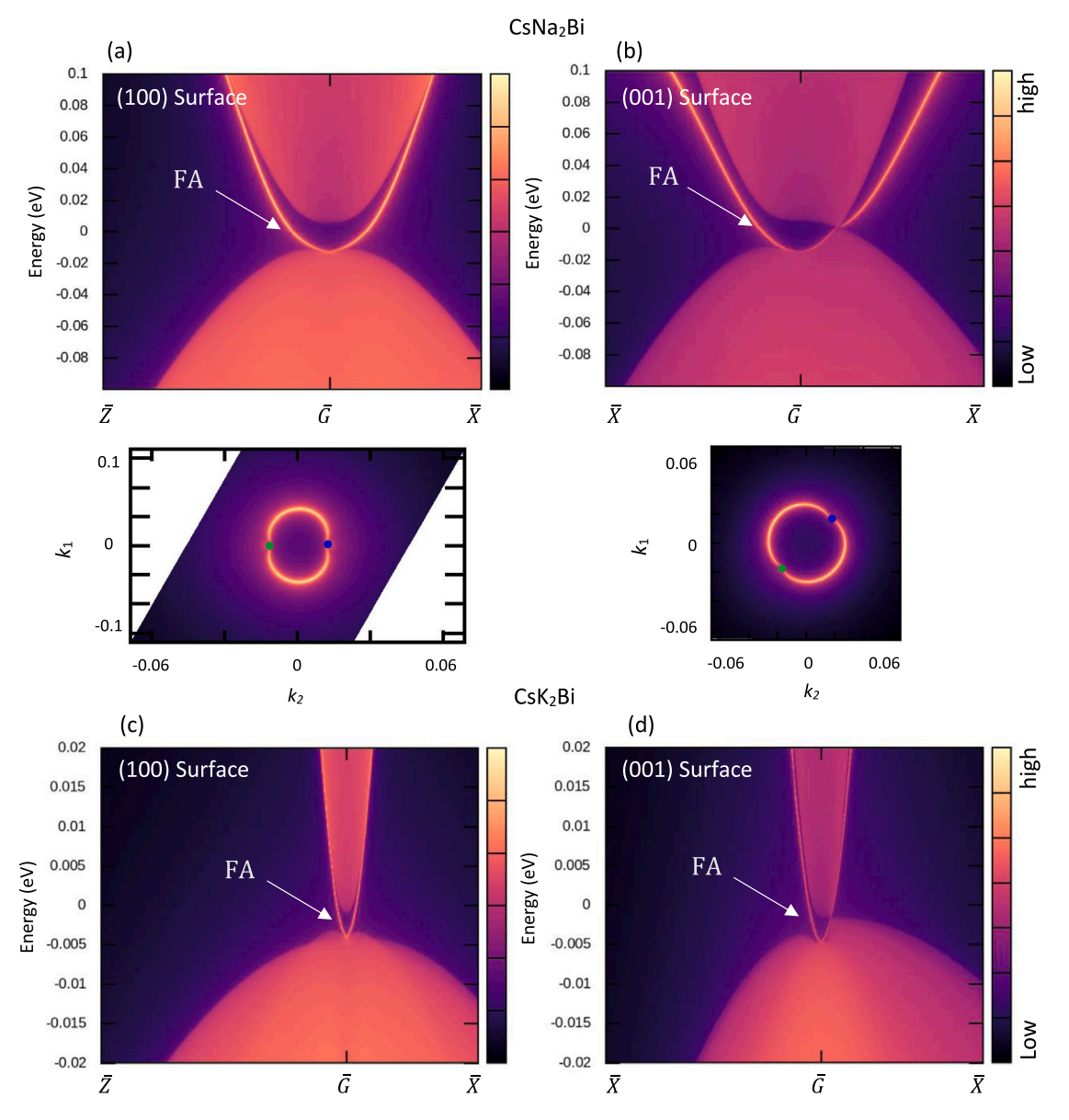


Fig. 12. The calculated TSS for the semi-infinite (a) (100) surface and (b) (001) surface of $CsNa_2Bi$ with SOC. The Fermi surface comprises two half-circle Fermi arcs terminated with two singular (Weyl) points (blue and green points) corresponding to the projection of bulk Dirac nodes. The calculated TSS for the semi-infinite (c) (100) surface and (d) (001) surface of CsK_2Bi in the presence of SOC. The Fermi surface for CsK_2Bi looks similar to that of $CsNa_2Bi$ and is not shown in the figure.

with Section 3.2. When m_0 is non-zero, the band degeneracy at the G point is lifted. It is noteworthy that when hydrostatic compression (Section 3.3) is applied to the system, the stability of the system in the topological semimetal phase is provided by the cubic symmetry and corresponds to $m_0=0$. In this case, all the basis orbitals are equivalent and have the same energy. When m_0 is non-zero, the band degeneracy at the G point is lifted. This is related to when the uniaxial strain is applied. Uniaxial tension (compression) strain corresponds to $m_0>0$ ($m_0<0$). When $m_0>0$ (see Fig. 14(a)), the system possesses a TWSM band structure with two Dirac/Weyl points located at $k=(0,0,\pm(m_0/m_1)^{1/2})$. When $m_0<0$ (see Fig. 14(c)), the system possesses a TI band structure with a nontrivial bandgap.

Finally, a summary of the effects of strain on the topological phases of these compounds when considering the spin-orbit coupling is shown schematically in Fig. 15. To the right of the figure due to the uniaxial tension, there is still band inversion, and Weyl points and Fermi Arcs are created on the (100) or (001) surfaces. According to the band structure, these Weyl points are of Type-I. Under compression strain TI phase with a non-trivial band gap is formed, shown on the left of the

figure. The presence of topological surface states (TSS) on (100) and (001) surfaces confirms this topological phase. By applying hydrostatic pressure, the compounds become conventional insulator with trivial band gap. Therefore, by changing the type of strain, these compounds can switch to various phases with different topological signatures.

4. Summary and outlook

In summary, we investigate the new full Heusler order compounds, CsM_2Bi (M = Na, K), with strain driven tunable topological states. We calculated the phonon dispersion and electronic properties of these structures under various types of strains. The topological band structures of these compounds were systematically investigated. It was found that both compounds possess different topological states, which can be effectively tuned by strain engineering. In the equilibrium state, *i.e.*, $V/V_0 = 1$ (no strain), the TS, TNSM, and NI classes appear in these compounds, which are calculated using both GGA and HSE06 approximations in the presence and absence of SOC. When the SOC is not considered in the calculations, the $CsNa_2Bi$ compound in both

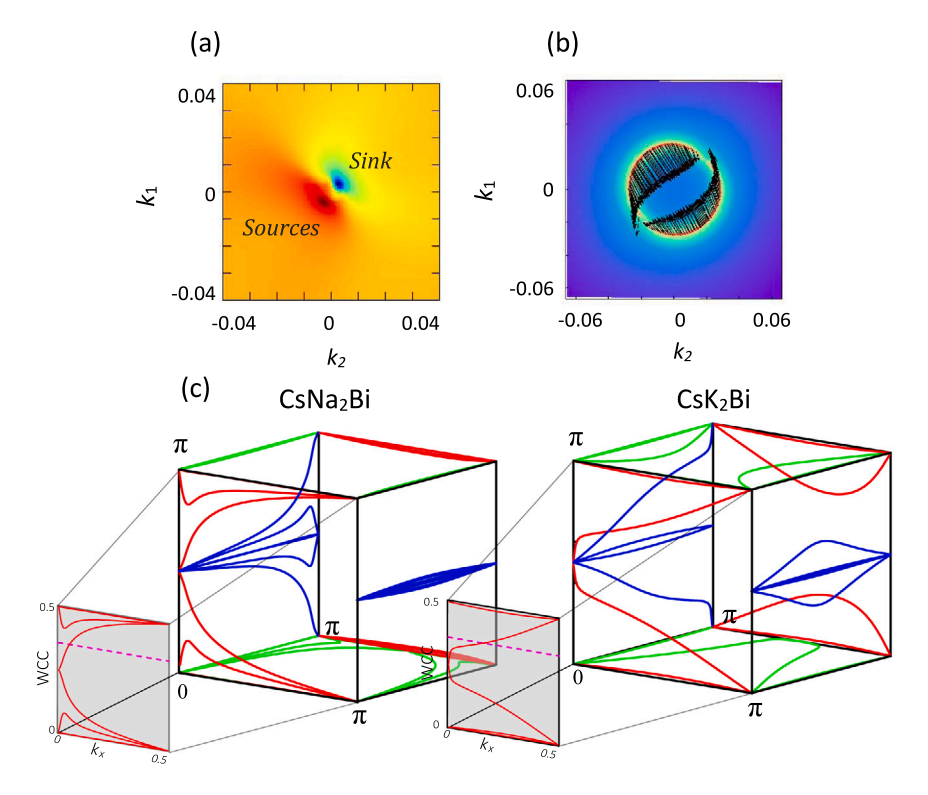


Fig. 13. (a) The Berry curvature and (b) Spin texture of CsNa₂Bi in the k_1 - k_2 (k_x - k_y) plane at the Fermi level of CsNa₂Bi. The source and sink points are the Weyl points with positive and negative chirality. The spin texture of the Fermi arcs has a helical behavior, for which the value of spin is not defined at the Weyl points. (c) Time reversal invariant cube (TRIC) in the presence of SOC. The WCC evolution for CaM₂Bi compounds on six time-reversal invariant momentum plane, k_x = 0, π (red color), k_y = 0, π (blue color) and k_z = 0, π (green color). (For interpretation of the references to color in this figure legend, the reader is referred to the web version of this article.)

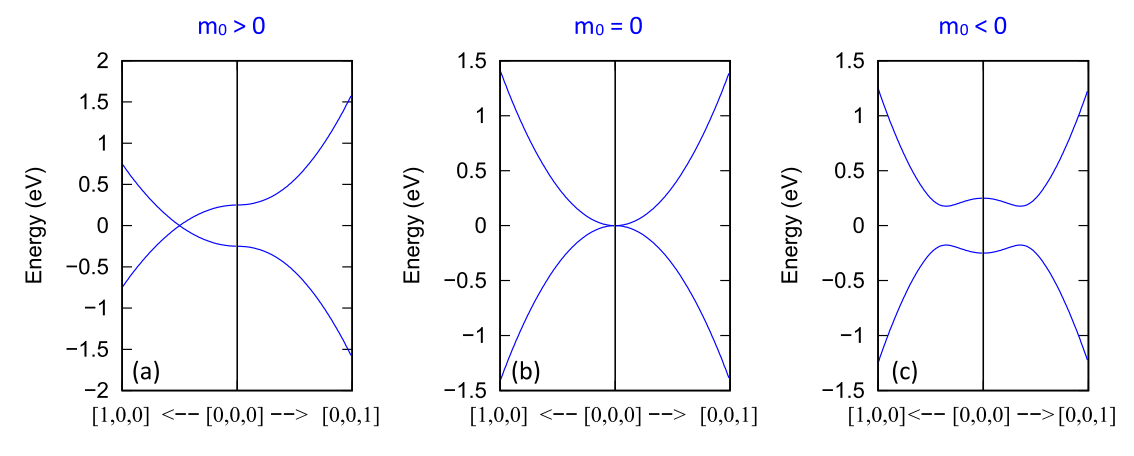


Fig. 14. Band dispersions obtained from H(k) by the low-energy effective k-p model with (a) $m_0 > 0$, (b) $m_0 = 0$ and (c) $m_0 < 0$. When $m_0 = 0$, the compound is a zero-gap semimetal. When $m_0 > 0$, the system possesses a TWSM band structure with two Weyl points. When $m_0 < 0$, the system possesses a TI band structure with a nontrivial bandgap.

approximations still shows nontrivial topological phases, although by applying a hydrostatic compression (V/V $_0\approx0.85$ for CsN $_2$ Bi and V/V $_0\approx0.94$ for CsK $_2$ Bi), a trivial phase is seen in both CsN $_2$ Bi and CsK $_2$ Bi structures. When SOC is considered in the computations, under uniaxial tension, both compounds are converted into a Weyl semimetal with nontrivial Fermi arcs on the surface; while applying a uniaxial compression leads to converting to the nontrivial topological insulating phase in both structures. These results offer diverse perspectives for multi-purpose applications of FHO CsM $_2$ Bi compounds as they host a diverse set of topological classes besides the well-known semiconducting properties. Finally, we suggest that biaxial strain may induce other interesting topological classes with practical implications in these compounds, which deserves further studies.

Declaration of competing interest

The authors declare that they have no known competing financial interests or personal relationships that could have appeared to influence the work reported in this paper.

Acknowledgments

This study is partially based upon work supported by the National Science Foundation (NSF), USA under grant numbers CBET-2110603 and ECCS-1711253.

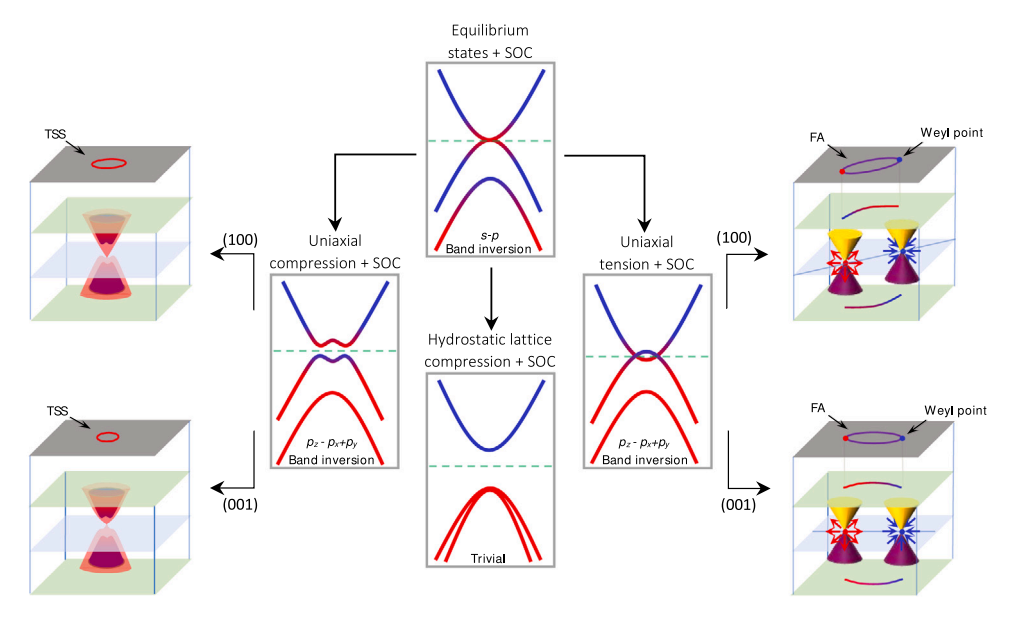


Fig. 15. Schematic of the band structure, band inversion, and topological surface states when the spin-orbit coupling is considered. In the right of the figure, there is still band inversion due to the uniaxial tension + SOC, and Weyl points and Fermi arcs (FA) are created on the (100) and (001) surface. According to the band structure, these Weyl points are of Type-I. To the left of the figure, under compression strain + SOC, TI phase with a non-trivial band gap is attained. The presence of TSS on (100) and (001) surfaces also confirms this topological phase. By applying hydrostatic pressure, the compounds become conventional insulators with trivial band gaps.

References

- [1] M.M.H. Polash, S. Yalameha, H. Zhou, K. Ahadi, Z. Nourbakhsh, D. Vashaee, Mater. Sci. Eng. R 145 (2021) 100620, https://doi.org/10.1016/j.mser.2021. 100620.
- [2] R.B. Laughlin, Phys. Rev. B 23 (10) (1981) 5632, https://doi.org/10.1103/ PhysRevB.23.5632.
- [3] Z. Liu, B. Zhou, Y. Zhang, Z. Wang, H. Weng, D. Prabhakaran, S.K. Mo, Z. Shen, Z. Fang, X. Dai, et al., Science 343 (6173) (2014) 864–867, https://www.science.org/lookup/doi/10.1126/science.1245085.
- [4] S. Yalameha, P. Saeidi, Z. Nourbakhsh, A. Vaez, A. Ramazani, J. Appl. Phys. 127 (8) (2020) 085102, https://doi.org/10.1063/1.5125920.
- [5] M. Narimani, S. Yalameha, Z. Nourbakhsh, J. Phys.: Condens. Matter 32 (25) (2020) 255501, https://doi.org/10.1088/1361-648X/ab6046.
- [6] J.C. Teo, L. Fu, C. Kane, Phys. Rev. B 78 (4) (2008) 045426, https://link.aps. org/doi/10.1103/PhysRevB.78.045426.
- [7] S. Singh, I. Valencia-Jaime, O. Pavlic, A.H. Romero, Phys. Rev. B 97 (5) (2018) 054108, https://link.aps.org/doi/10.1103/PhysRevB.97.054108.
- [8] W. Feng, D. Xiao, J. Ding, Y. Yao, Phys. Rev. Lett. 106 (2011) 016402, https://link.aps.org/doi/10.1103/PhysRevLett.106.016402.
- [9] S. Yalameha, Z. Nourbakhsh, A. Vaez, J. Magn. Magn. Mater. 468 (2018) 279–286, https://doi.org/10.1016/j.jmmm.2018.07.086.
- [10] X.-L. Sheng, Z. Wang, R. Yu, H. Weng, Z. Fang, X. Dai, Phys. Rev. B 90 (2014) 245308, https://link.aps.org/doi/10.1103/PhysRevB.90.245308.
- [11] N. Armitage, E. Mele, A. Vishwanath, Rev. Modern Phys. 90 (1) (2018) 015001, https://link.aps.org/doi/10.1103/RevModPhys.90.015001.
- [12] T. Wehling, A.M. Black-Schaffer, A.V. Balatsky, Adv. Phys. 63 (1) (2014) 1–76, https://doi.org/10.1080/00018732.2014.927109.
- [13] S.A. Yang, Spin, 6, (02) World Scientific, 2016, 1640003, https://doi.org/10. 1142/S2010324716400038.
- [14] L. Jin, X. Zhang, T. He, W. Meng, X. Dai, G. Liu, Phys. Chem. Chem. Phys. 22 (10) (2020) 5847–5854. https://doi.org/10.1039/C9CP06033B.
- [15] J. Ruan, S.-K. Jian, H. Yao, H. Zhang, S.-C. Zhang, D. Xing, Nature Commun. 7 (1) (2016) 1–6, https://www.nature.com/articles/ncomms11136.
- [16] J. Ruan, S.-K. Jian, D. Zhang, H. Yao, H. Zhang, S.-C. Zhang, D. Xing, Phys. Rev. Lett. 116 (2016) 226801, https://link.aps.org/doi/10.1103/PhysRevLett. 116.226801.
- [17] S.-Y. Yang, H. Yang, E. Derunova, S.S. Parkin, B. Yan, M.N. Ali, Adv. Phys. X 3 (1) (2018) 1414631, https://doi.org/10.1080/23746149.2017.1414631.
- [18] X. Zhang, L. Jin, X. Dai, G. Liu, J. Phys. Chem. Lett. 8 (19) (2017) 4814–4819, https://doi.org/10.1021/acs.jpclett.7b02129.
- [19] S. Yalameha, Z. Nourbakhsh, J. Phys.: Condens. Matter 32 (29) (2020) 295502, https://doi.org/10.1088/1361-648X/ab80f4.
- [20] W. Meng, X. Zhang, T. He, L. Jin, X. Dai, G. Liu, J. Phys. Chem. C 124 (13) (2020) 7378–7385, https://doi.org/10.1021/acs.jpcc.0c00303.
- [21] R. Yu, Q. Wu, Z. Fang, H. Weng, Phys. Rev. Lett. 119 (3) (2017) 036401, https://link.aps.org/doi/10.1103/PhysRevLett.119.036401.

- [22] S.-Y. Xu, I. Belopolski, N. Alidoust, M. Neupane, G. Bian, C. Zhang, R. Sankar, G. Chang, Z. Yuan, C.-C. Lee, et al., Science 349 (6248) (2015) 613–617, https://www.science.org/doi/full/10.1126/science.aaa9297.
- [23] T. Nomoto, H. Ikeda, J. Phys. Soc. Japan 86 (2) (2017) 023703, https://doi.org/ 10.7566/JPSJ.86.023703.
- [24] G. Bian, T.-R. Chang, R. Sankar, S.-Y. Xu, H. Zheng, T. Neupert, C.-K. Chiu, S.-M. Huang, G. Chang, I. Belopolski, et al., Nature Commun. 7 (1) (2016) 1–8, https://doi.org/10.1038/ncomms10556.
- [25] L. Šmejkal, T. Jungwirth, J. Sinova, Phys. Status Solidi (RRL)–Rapid Res. Lett. 11 (4) (2017) 1700044, https://doi.org/10.1002/pssr.201770317.
- [26] G. Liu, L. Jin, X. Dai, G. Chen, X. Zhang, Phys. Rev. B 98 (7) (2018) 075157, https://link.aps.org/doi/10.1103/PhysRevB.98.075157.
- [27] T.-T. Zhang, Z.-M. Yu, W. Guo, D. Shi, G. Zhang, Y. Yao, J. Phys. Chem. Lett. 8 (23) (2017) 5792–5797, https://doi.org/10.1021/acs.jpclett.7b02642.
- [28] Z. Wang, D. Gresch, A.A. Soluyanov, W. Xie, S. Kushwaha, X. Dai, M. Troyer, R.J. Cava, B.A. Bernevig, Phys. Rev. Lett. 117 (5) (2016) 056805, https://link. aps.org/doi/10.1103/PhysRevLett.117.056805.
- [29] S. Li, Z.-M. Yu, Y. Liu, S. Guan, S.-S. Wang, X. Zhang, Y. Yao, S.A. Yang, Phys. Rev. B 96 (8) (2017) 081106, https://link.aps.org/doi/10.1103/PhysRevB.96. 081106
- [30] X.-L. Sheng, Z.-M. Yu, R. Yu, H. Weng, S.A. Yang, J. Phys. Chem. Lett. 8 (15) (2017) 3506–3511, https://doi.org/10.1021/acs.jpclett.7b01390.
- [31] F. Shang, G. Wang, Comput. Mater. Sci. 160 (2019) 275–278, https://doi.org/ 10.1016/j.commatsci.2018.12.047.
- [32] A. Narayan, D. Di Sante, S. Picozzi, S. Sanvito, Phys. Rev. Lett. 113 (25) (2014) 256403, https://link.aps.org/doi/10.1103/PhysRevLett.113.256403.
- [33] A. Ebrahimian, R. Asgari, M. Dadsetani, Phys. Rev. B 102 (16) (2020) 165119, https://link.aps.org/doi/10.1103/PhysRevB.102.165119.
- [34] T. Zhang, Y. Jiang, Z. Song, H. Huang, Y. He, Z. Fang, H. Weng, C. Fang, Nature 566 (7745) (2019) 475–479, https://doi.org/10.1038/s41586-019-0944-6.
- [35] M. Vergniory, L. Elcoro, C. Felser, N. Regnault, B.A. Bernevig, Z. Wang, Nature 566 (7745) (2019) 480–485, https://doi.org/10.1038/s41586-019-0954-4.
- [36] F. Tang, H.C. Po, A. Vishwanath, X. Wan, Nature 566 (7745) (2019) 486–489, https://doi.org/10.1038/s41586-019-0937-5.
- [37] S.M. Young, S. Chowdhury, E.J. Walter, E.J. Mele, C.L. Kane, A.M. Rappe, Phys. Rev. B 84 (8) (2011) 085106, https://link.aps.org/doi/10.1103/PhysRevB.84. 085106.
- [38] J. Liu, Y. Xu, J. Wu, B.-L. Gu, S. Zhang, W. Duan, Acta Crystallogr. C 70 (2) (2014) 118–122, https://doi.org/10.1107/S2053229613032336.
- [39] Y. Nie, M. Rahman, D. Wang, C. Wang, G. Guo, Sci. Rep. 5 (1) (2015) 1–6, https://doi.org/10.1038/srep17980.
- [40] C. Zhao, M. Hu, J. Qin, B. Xia, C. Liu, S. Wang, D. Guan, Y. Li, H. Zheng, J. Liu, et al., Phys. Rev. Lett. 125 (4) (2020) 046801, https://link.aps.org/doi/10. 1103/PhysRevLett.125.046801.
- [41] P. Blaha, K. Schwarz, F. Tran, R. Laskowski, G.K. Madsen, L.D. Marks, J. Chem. Phys. 152 (7) (2020) 074101, https://doi.org/10.1063/1.5143061.
- [42] J.P. Perdew, K. Burke, M. Ernzerhof, Phys. Rev. Lett. 77 (18) (1996) 3865, https://link.aps.org/doi/10.1103/PhysRevLett.77.3865.

- [43] J. Heyd, G.E. Scuseria, J. Chem. Phys. 121 (3) (2004) 1187–1192, https://doi. org/10.1063/1.1760074.
- [44] G. Pizzi, V. Vitale, R. Arita, S. Blügel, F. Freimuth, G. Géranton, M. Gibertini, D. Gresch, C. Johnson, T. Koretsune, et al., J. Phys.: Condens. Matter 32 (16) (2020) 165902, https://doi.org/10.1088/1361-648X/ab51ff.
- [45] M.L. Sancho, J.L. Sancho, J. Rubio, J. Physics F Met. Phys. 15 (4) (1985) 851, https://doi.org/10.1088/0305-4608/15/4/009.
- [46] A. Togo, I. Tanaka, Scr. Mater. 108 (2015) 1–5, https://doi.org/10.1016/j. scriptamat.2015.07.021.
- [47] M. Jamal, M. Bilal, I. Ahmad, S. Jalali-Asadabadi, J. Alloys Compd. 735 (2018) 569–579, https://doi.org/10.1016/j.jallcom.2017.10.139.
- [48] M. Born, K. Huang, Dynamical Theory of Crystal Lattices, Clarendon Press, 1954.
- [49] C. Oses, (Ph.D. thesis), Duke University, 2018.
- [50] A.M. Essin, V. Gurarie, Phys. Rev. B 84 (12) (2011) 125132, https://link.aps. org/doi/10.1103/PhysRevB.84.125132.

- [51] L. Fu, C.L. Kane, Phys. Rev. B 76 (4) (2007) 045302, https://link.aps.org/doi/ 10.1103/PhysRevB.76.045302.
- [52] A.A. Soluyanov, D. Vanderbilt, Phys. Rev. B 83 (23) (2011) 235401, https://link.aps.org/doi/10.1103/PhysRevB.83.235401.
- [53] A. Mashmool, P. Saeidi, S. Yalameha, Z. Nourbakhsh, J. Magn. Magn. Mater. 503 (2020) 166572, https://doi.org/10.1016/j.jmmm.2020.166572.
- [54] A. Narayan, J. Phys. Chem. Solids 128 (2019) 231–236, https://doi.org/10.1016/ j.jpcs.2017.10.035.
- [55] P. Zhou, Z. Ma, L. Sun, J. Mater. Chem. C 6 (5) (2018) 1206–1214, https://doi.org/10.1039/C7TC05095J.
- [56] I.Y. Sklyadneva, I.P. Rusinov, R. Heid, K.-P. Bohnen, P.M. Echenique, E.V. Chulkov, Sci. Rep. 6 (2016) 24137, https://doi.org/10.1038/srep24137.
- [57] A.A. Soluyanov, D. Gresch, Z. Wang, Q. Wu, M. Troyer, X. Dai, B.A. Bernevig, Nature 527 (7579) (2015) 495–498, https://doi.org/10.1038/nature15768.
- [58] Z. Fang, N. Nagaosa, K.S. Takahashi, A. Asamitsu, R. Mathieu, T. Ogasawara, H. Yamada, M. Kawasaki, Y. Tokura, K. Terakura, Science 302 (5642) (2003) 92–95, https://www.science.org/doi/abs/10.1126/science.1089408.